Unconventional Resources 16 (2027) 100469

Contents lists available at ScienceDirect

Unconventional Resources

journal homepage: www.keaipublishing.com/en/journals/unconventional-resources/

Designing wave farms to support mangrove restoration: A coupled hydro-morphodynamic and habitat suitability modelling approach

Avinash Boodoo [a,*], Deborah Villarroel-Lamb [b], Jeffrey S. Cross [a]

[a] Department of Transdisciplinary Science and Engineering, School of Environment and Society, Institute of Science Tokyo, Meguro, Tokyo, 152-8550, Japan

[b] Department of Civil and Environmental Engineering, Faculty of Engineering, The University of the West Indies, West Indies, St. Augustine, Trinidad and Tobago

ARTICLE INFO

Keywords:
Wave farms
Mangrove restoration
Morphodynamics
Wave energy
Renewable energy

ABSTRACT

Wave farms are increasingly proposed for hybrid coastal infrastructure, offering both renewable energy generation and shoreline protection. However, their potential to enable ecological restoration, particularly for mangrove restoration, remains underexplored. This study presents a novel framework for evaluating how wave farms can precondition coastal zones for mangrove restoration by attenuating wave energy, reducing erosion, and expanding areas of hydrodynamic suitability. Using a schematized coupled depth averaged (2DH) hydrodynamic, spectral wave and morphodynamic model in Delft3D, six wave farm configurations were tested under idealized conditions to quantify wave attenuation, sediment retention, and habitat suitability. Mangrove survivability was assessed through a novel drag-based (Type II) erosion-adjusted uprooting threshold. K-means clustering was applied to field-collected morphological traits to define three distinct seedling groups, enabling species-specific resistance modelling based on frontal area and anchorage. The results show that array layout strongly influences ecological and engineering performance. Some configurations enhanced erosion reduction and created more contiguous planting zones while others expanded the total area suitable for restoration. The proposed framework identifies zones preconditioned for restoration, which can be made viable for planting through interventions such as mud nourishment or raised platforms. This study provides a transferable methodology to support hybrid infrastructure design for climate resilience, ecosystem recovery, and local socioeconomic benefit.

1. Introduction

Traditional coastal protection strategies such as seawalls, revetments, and breakwaters have long been used to defend coastlines from coastal hazards such as erosion and flooding. However, these hard-engineering approaches can be ecologically disruptive, expensive to maintain, and maladaptive in the face of climate change and sea level rise [1–4]. In response, there is growing interest in Nature-Based Solutions (NbS) and Eco-Engineering; strategies that leverage the adaptive capacity of natural ecosystems to reduce coastal hazards while delivering essential ecosystem services and co-benefits such as habitat restoration and carbon sequestration [3–5].

Among NbS, mangroves are particularly valuable due to their ability to attenuate wave energy, reduce current velocities, trap sediments, and stabilize intertidal substrates [6–9]. Multiple field and modelling studies have shown that even narrow mangrove belts can significantly reduce wave height and storm surges [10–14]. However, despite their promise, mangrove restoration projects often suffer from low survival and establishment rates, particularly in high-energy environments. This is often due to excessive hydrodynamic forces that exceed the mechanical anchorage capacity of young seedlings, leading to uprooting or burial before the root system can establish [15–20].

To address this, hybrid solutions have been proposed that combine nature-based elements like mangroves with engineered structures such as submerged breakwaters, permeable dams and bamboo fences among others [21–24]. These structures aim to reduce incoming wave energy to tolerable levels and promote sediment deposition in front of the mangrove planting zone [16,21,22,24–26]. While this approach has shown promise in improving seedling survival, it presents several limitations: breakwaters are costly to construct, rigid in design, and difficult to relocate, potentially restricting the natural seaward migration of mangrove forests resulting in coastal squeeze [27]. These structures are

Peer review under the responsibility of KeAi Communications Co., Ltd.

* Corresponding author.
E-mail address: boodoo.a.aa@m.titech.ac.jp (A. Boodoo).

https://doi.org/10.1016/j.uncres.2026.100469
Received 8 March 2026; Received in revised form 15 June 2026; Accepted 15 June 2026
Available online 18 June 2026

typically single-purpose and non-adaptive and may become increasingly ineffective under scenarios of progressive sea level rise. Moreover, generating spatial planting suitability maps remains challenging because field-based morphological proxies for anchorage are difficult to generalize, owing to variability in root development and the practical limitations of measuring subsurface traits non-destructively.

An emerging opportunity lies in the dual use of Wave Energy Converters (WECs) and wave farms to support the development and growth of mangrove seedlings while providing renewable energy. Wave energy is increasingly being recognized as a promising renewable resource that can help meet growing global energy demands while supporting carbon neutral power generation [28–33]. The dual use of WECs and wave farms has been proposed as a solution to reduce the high Levelized Cost of Electricity (LCoE) as well as provide renewable energy and coastal protection [32,34–37] Wave farms have proven to be able to reduce wave heights by 10% to 50% and erosion by 15% to 45%, depending on factors such as location and wave conditions, WEC array layout, device spacing and distance from the shore [32,34,38–43]. To the authors' knowledge, such a hybrid approach combining ecological restoration with technological infrastructure such as WECs has not yet been proposed in the scientific literature, despite its potential relevance to remote, energy-poor, erosion-prone, and vulnerable coastal regions.

This study addresses this gap by integrating numerical modelling with a data-driven anchorage framework to evaluate the spatial survivability of mangrove seedlings under different wave farm scenarios. The anchorage data from Kibler et al. [18], comprising over 180 mangrove seedlings with measured morphological traits and pull-out resistance was incorporated. Using K-means clustering, seedlings are grouped into morphological classes, each assigned a group-specific resistance threshold. A schematized, coupled depth-averaged (2DH) hydrodynamic, spectral wave, and morphodynamic model is implemented in Delft3D, using simplified bathymetry and idealized forcing conditions to represent an idealized wave-exposed fine-grained coastal restoration frontage for testing WEC-assisted hydrodynamic preconditioning under controlled conditions. Model parameters reflect typical environmental ranges observed in restoration sites, including wave heights, sediment characteristics, and water depths. The group-specific thresholds are then combined with erosion and drag force outputs from Delft3D to generate spatially explicit maps of seedling survivability under both baseline and WEC-deployed scenarios.

Although the modelled suitability zones in this study fall deeper than the intertidal elevations typically required for mangrove establishment, similar conditions have been successfully converted into restoration-ready land using sedimentation-enhancing strategies (SES). A recent global synthesis by Cox et al. [44] found that SES such as tidal flooding, sediment diversions, and permeable sedimentation structures have effectively raised bed elevations in deltas worldwide by 1–2 m. Notably, these strategies often target low-lying or submerged areas and rely on calm hydrodynamic conditions to allow sediment deposition. In this study, the WECs serve as wave-attenuating structures that create such calm zones, preconditioning deeper areas for restoration. These zones could then be elevated through site preparation interventions such as mud nourishment or passive sediment accumulation, consistent with SES frameworks documented in field-scale delta restoration projects [44].

By linking device layout to ecological outcomes, this study offers a novel hybrid nature-technology framework for enhancing coastal resilience while supporting local restoration efforts and renewable energy generation. From a climate resilient coastal engineering perspective, the integration of wave farms with mangrove ecosystem restoration represents a potential pathway toward multifunctional coastal infrastructure. Unlike conventional hard structures that primarily provide static protection, wave farms can be configured to modify hydrodynamic and morphodynamic processes while also supporting renewable energy generation. When combined with mangrove restoration, these hydrodynamic and morphodynamic effects may help create more stable preconditioning zones where wave forcing and erosion are reduced before planting or sediment-enhancement interventions are implemented. Such hybrid systems are particularly relevant under climate change and sea level rise pressures, where coastal protection strategies must increasingly combine engineering performance, ecological recovery, adaptability, and socioeconomic co-benefits. In this context, the present study evaluates how WEC array layout influences hydro-morphodynamic interactions and seedling survivability thresholds, providing an exploratory framework for climate-resilient coastal design.

The specific objectives of this study are: (i) to use published morphological and anchorage data to classify seedlings into morphological groups and assign rooting depth and resistance thresholds; (ii) to model wave attenuation and sediment dynamics under varying WEC configurations using Delft3D; (iii) to develop an erosion-adjusted anchorage model that incorporates rooting depth loss and wave drag; and (iv) to generate spatial habitat suitability maps for different seedling types under baseline and wave farm conditions.

The remainder of this paper is structured as follows: Section 2 describes the data source, classification methodology, and Delft3D model setup. Section 3 presents the anchorage grouping results, wave attenuation outputs, and habitat suitability maps. Section 4 discusses the implications and limitations of the hybrid wave farm–mangrove framework. Section 5 concludes with recommendations for future applications and research.

2. Methods

2.1. Data source and study species

In the field study, 182 seedlings (95 *R. mangle*, 87 *A. germinans*) were collected from mangrove forests at two estuarine sites in Florida: De Soto National Memorial (DESOTO) and Canaveral National Seashore (CANA). For the purposes of this study, only the 87 seedlings from the DESOTO site were used. The DESOTO field sites were characterized by organic-rich mangrove substrates, with organic matter content ranging from 10.4% to 56.4% and median grain sizes (D_{50}) ranging from 0.22 to 0.46 mm, corresponding primarily to fine-to medium-sand-sized material. Although these sediments are sand-sized based on median grain diameter, the high organic content, vegetation cover, and root-sediment interactions may contribute to cohesive-like or bio stabilized behaviour. In the present study, these sediment characteristics are reported as contextual information for the biological anchorage dataset and were not used to parameterize the Delft3D sediment model. Each seedling underwent lateral pull testing in situ, and the following morphological traits were recorded: aboveground biomass (AGB), belowground biomass (BGB), seedling height, basal diameter, number of leaves, and shoot frontal area. However, root length was not measured in the field. Additional site variables included groundcover vegetation density and canopy closure, which were measured using standard ecological field methods.

In the laboratory experiments, 180 propagules (90 per species) were grown for in controlled conditions using two artificial sediment types: one with whole oyster shells and one with crushed shells, both mixed with 50% commercial sand (no organic content). After growth, seedlings were uprooted using the same lateral pull methodology, and aboveground biomass, belowground biomass and root length were measured. This allowed for direct estimation of rooting depth, which was not available from the field dataset.

To ensure that model inputs reflected real-world resistance in cohesive substrates, only field-derived anchorage force values from the DESOTO site were used in the erosion-adjusted anchorage model. However, because the field dataset lacked root length measurements, rooting depth values were inferred from the lab-grown seedlings, which were grouped using the same morphology-based clustering approach (described in Section 2.2). Representative root lengths from each lab-based morphological group were then assigned to the corresponding field-based groups. This approach allowed us to define morphology-specific survivability thresholds that integrate field-based resistance with realistic rooting depth estimates, enabling spatial assessment of seedling stability across different hydrodynamic scenarios in the model domain.

The anchorage resistance values used in this study represent field-derived plant–substrate resistance of naturally established mangrove seedlings under the conditions measured by Kibler et al. [18]. They should not be interpreted as sediment-specific resistance values for a purely muddy substrate. Although Kibler et al. [18] did not detect a strong sediment-texture effect on anchoring force for field seedlings older than three months, anchorage resistance may vary with substrate type, consolidation, organic content, root architecture, and surrounding vegetation. Therefore, the values used here are interpreted as first-order morphology-specific anchorage thresholds for framework development, rather than site-calibrated resistance values for all muddy restoration environments.

It is important to note that the Florida mangrove dataset was not used to define the numerical model bathymetry, wave climate, or sediment forcing. Instead, the dataset was used only to parameterize the biological component of the framework, namely morphology-specific anchorage resistance, shoot frontal area, and estimated rooting depth. The Delft3D model was, therefore, not intended to reproduce the DESOTO or CANA sites. Rather, the biological thresholds derived from the mangrove seedling data were coupled with an idealized hydro-morphodynamic model to demonstrate how WEC-induced changes in wave forcing and erosion could be translated into spatial survivability indicators.

2.2. Morphology-based grouping of seedlings

To classify seedlings into morphology groups for spatial survivability analysis, a K-means clustering algorithm was applied to data collected from the field site. The objective of the clustering was to identify functionally distinct seedling types with different aboveground morphologies and anchorage resistance thresholds, which could be used to map survivability across the model domain.

Seedlings were grouped into three morphology classes using K-means clustering based on AGB and BGB. These two traits were selected as integrative indicators of seedling maturity and anchorage potential. AGB reflects the overall shoot development and wave drag exposure, while BGB correlates with root system size and mechanical resistance. Prior to clustering, values were standardized using z-score normalization, and cluster labels were reordered by ascending mean AGB to define small, medium, and large morphology groups:

$$z = \frac{x - \mu}{\sigma} \tag{1}$$

where x is the raw value, μ is the sample mean, and σ is the standard deviation.

2.2.1. Morphology-based grouping using K-means clustering

K-means clustering was implemented using the scikit-learn Python package. The number of clusters was set to three, representing "small," "medium," and "large" morphological groups. This choice was guided by visual inspection of trait distributions, ecological interpretability, and the elbow method. Each seedling was assigned to a morphology group, and group-level means were calculated for shoot traits and anchorage resistance, F_R (N).

Because the dataset did not include root length, rooting depth estimates were assigned to each morphology group based on corresponding cluster results from the lab dataset, where the longest root length was available. This allowed the rooting depth (z_0), to be approximated as an erosion threshold for each group, which was then integrated into the erosion-adjusted anchorage framework. Field-measured resistance values were paired with morphology-specific rooting depth estimates to evaluate where seedlings would survive or fail across the model domain, both with and without WEC array deployment.

2.3. Process-based numerical modelling

2.3.1. Model description

A process-based, depth-averaged (2DH) numerical model was developed using Delft3D to simulate coupled hydrodynamics, spectral wave transformation, sediment transport, and long-term morphodynamics of an idealized model domain. The model consists of three dynamically linked components: Delft3D-FLOW (hydrodynamics), Delft3D-WAVE, which is based on SWAN (Simulating WAves Nearshore), and the Morphology module.

An online coupling was implemented between Delft-FLOW and Delft-WAVE, enabling two-way interaction at each computational timestep. The wave module simulates the propagation of random, short-crested wind waves in coastal areas, accounting for depth-induced breaking, bottom friction, and wave–current interaction. Radiation stress gradients computed in the wave module are passed to the hydrodynamic model to influence flow patterns and sediment mobility. Conversely, time-varying water levels and flow velocities from the FLOW module are used to update wave propagation and energy dissipation in Delft-WAVE. The Morphology module was activated to simulate bathymetric changes driven by both wave- and current-induced sediment transport.

2.3.1.1. Hydrodynamic model. The hydrodynamic model, Delft3D-FLOW, solves the unsteady Shallow Water Equations (SWE), which include the horizontal momentum and continuity equations, using a finite difference scheme on a structured grid [45]. These equations describe conservation of mass and momentum under the hydrostatic and depth-averaged assumptions and are the standard governing equations implemented in Delft3D-FLOW for two-dimensional coastal and shallow-water applications. The model is forced at open boundaries by tidal and meteorological inputs and is widely used to simulate flow dynamics in coastal and shallow marine environments. It computes depth-averaged flow velocities and water level variations in response to tidal forcing, pressure gradients, and bed friction. Delft3D-FLOW is particularly well suited for resolving nearshore current patterns that influence sediment transport, and in this study, it provides the hydrodynamic foundation for the coupled modelling of long-term morphodynamic change.

2.3.1.2. Spectral wave model. The spectral wave module, Delft3D-WAVE, is based on the SWAN model, which solves the spectral action balance equation (Equation (2)) to simulate the propagation and transformation of random, short-crested wind waves in coastal and nearshore environments. It accounts for processes including wave generation by wind, whitecapping, depth-induced breaking, bottom friction, shoaling, refraction, and nonlinear wave–wave interactions.

$$\frac{\partial N}{\partial t} + \nabla_{\vec{x}} \cdot \left[\left(\vec{c_g} + \vec{u} \nabla \right) N \right] + \frac{\partial c_\sigma N}{\partial \sigma} + \frac{\partial c_\theta N}{\partial \theta} = \frac{S_{tot}}{\sigma} \tag{2}$$

This equation governs the evolution of wave action density $N(\sigma, \theta)$ in time, space, frequency, and direction. The first term represents the local rate of change of wave action; the second term captures spatial propagation driven by wave group velocity $\vec{c_g}$ and ambient currents $\vec{u}$. The third and fourth terms represent shifts in frequency and direction due to shoaling and refraction. The right-hand side, $\frac{S_{tot}}{\sigma}$, represents the net source term, incorporating wind input, whitecapping, bottom friction, depth-induced breaking, and nonlinear interactions. Model inputs include bathymetric data, wave and wind data. Key physical processes such as whitecapping, bottom friction, and wave breaking were activated.

2.3.1.3. Morphodynamic model. The morphodynamic component of the model was implemented using the Morphology module in Delft3D-FLOW. This module computes bed level changes over time by solving the Exner equation for sediment continuity, which accounts for gradients in sediment transport driven by hydrodynamic flows and wave forcing. The model is run in depth-averaged (2DH) mode, and morphological updates are applied at each hydrodynamic time step using the Exner equation:

$$\frac{\partial z_b}{\partial t} + \frac{1}{1-p}\nabla \cdot \vec{q_s} = 0 \quad (3)$$

Where z_b is the bed level elevation, p is the sediment porosity, and $\vec{q_s}$ is the total sediment transport vector (bedload + suspended load). To simulate long-term seabed evolution efficiently, a morphological scale factor, commonly referred to in Delft3D as MORFAC, is applied, which scales up the rate of bed level change relative to hydrodynamic time. In Delft3D, the MORFAC is applied during the bed-level update by multiplying the computed bed-level change at each hydrodynamic time step. Therefore, MORFAC does not modify the hydrodynamic or sediment transport equations directly; rather, it scales the rate of morphological change relative to the simulated hydrodynamic time.

2.3.2. Model set-up

A schematized 2DH coupled hydrodynamic, spectral wave, and sediment transport model was developed in Delft3D to simulate wave attenuation and morphodynamic changes with and without WECs. This idealized modelling approach was selected to isolate the fundamental interactions between WECs, wave dynamics, and sediment transport in a controlled environment, free from the complexities of site-specific bathymetry or forcing. Such schematized models are widely used in early-stage or exploratory research, especially when field data are limited or unavailable, or when the objective is to compare alternative configurations (e.g., WEC layouts, sediment types, or beach slopes).

The Delft3D model was not intended to reproduce a specific field site or the Florida locations from which the mangrove seedling anchorage data were obtained. Instead, the biological dataset was used to parameterize morphology-specific anchorage resistance, shoot frontal area, and rooting depth thresholds, while the numerical model represents an idealized wave-exposed fine-grained coastal restoration frontage. The model should therefore be interpreted as a proof-of-concept framework for testing WEC-assisted hydrodynamic preconditioning, rather than as a site-specific prediction of mangrove restoration success.

In estuarine environments, morphodynamic evolution typically unfolds over multi-year timescales, making field validation and long-term simulation particularly challenging and computationally intensive [46,47]. The use of a schematized domain in this study, rather than a real-world site, allowed for efficient yet representative modelling of wave–sediment processes under conditions characteristic of muddy estuarine zones suitable for mangrove restoration. This method is commonly adopted in coastal morphodynamic research to examine long-term sediment behaviour and isolate key process drivers under simplified but realistic conditions [46–54]. All model parameters including sediment properties, wave forcing, erosion thresholds, and WEC parameters were defined using literature values appropriate for cohesive sediment environments and is summarised in Table 1.

The model domain was idealized, consisting of a 1000 m × 1000 m grid discretized into 80 × 40 structured cells, with cross-shore (X-direction) grid spacing of 12.5 m and alongshore (Y-direction) spacing of 25 m. Bathymetry was defined using a uniform 1:80 slope extending from the shoreline to the seaward boundary at 12.5 m water depth (Fig. 1). This slope is steeper than many low-gradient muddy mangrove flats, which often develop on broad intertidal platforms. However, comparable bed slopes have been reported or adopted in previous mangrove-related coastal studies, particularly for wave-exposed or restoration-oriented settings where hydrodynamic forcing and shoreline transition processes are important [27,55]. In the present study, the 1:80

Table 1
Summary of Delft3D model parameters.

Parameter	Value	Source
Model Type	Delft3D (2DH) Hydrodynamic + Wave + Morphology	-
Grid Dimensions	1000 m × 1000 m	-
Grid Resolution	80 × 40 cells (12.5 m × 25 m)	-
Bathymetry	Idealized 1:80 slope with maximum 12.5 m depth	Risheharan et al. [27]; Gijsman et al. [55]
WEC Representation	Obstacles, 12.5 m width, 25 m gap (2D spacing), K_t = 0.2, K_r = 0.8	Boodoo et al. [32]
WEC Location	500 m offshore	-
Tidal Forcing	M2 and S2 constituents (0.35 m tidal range)	Hashim et al. [21]; Winterwerp et al. [24]
Wave Forcing	H_{sig} = 1 m, T_p = 8 s, D_m = 10°	Hashim et al. [21]; Winterwerp et al. [24]
Sediment Type	Cohesive sediment	-
Sediment Properties	ρ = 2650 kg/m^3, dry bed ρ = 500 kg/m^3, settling velocity = 0.1 mm/s, τ_{ce} = 0.4 N/m^2, τ_{cd} = 0.05 N/m^2	Delft3D-FLOW User Manual; Borsje et al. [56]; He et al. [46];
Simulation Duration	1 Jan 2025 – 31 Jan 2025	-
Morphological Scale Factor (MORFAC)	10	-

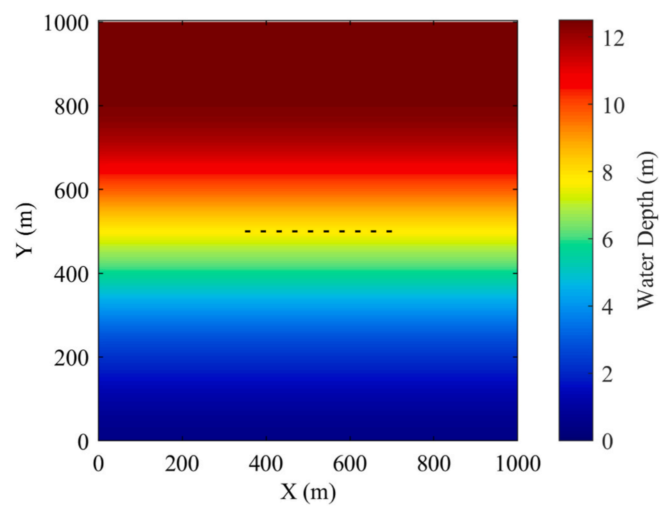

Fig. 1. Idealized model bathymetry and WEC array placement for the base configuration. The black segments indicate the 2D WEC array located 500 m from the shoreline, with 10 idealized bottom-mounted oscillating wave surge converter-type devices similar to devices like the WaveRoller. The WECs were represented in Delft3D as partially reflective and transmissive obstacles using K_t = 0.2 and K_r = 0.8.

profile is therefore not intended to represent all muddy mangrove coastlines, but rather a simplified wave-exposed transition profile seaward of potential mangrove restoration areas. This simplified bathymetry was retained to resolve wave shoaling, WEC-induced wave attenuation, and bed response within a controlled 1 km model domain, while allowing direct comparison among WEC layouts without site-specific bathymetric complexity.

Hydrodynamic forcing was applied through the FLOW module using a tidal boundary condition at the northern Open boundary. The astronomic tidal signal was represented using the primary M2 and S2 constituents, prescribed to produce a semidiurnal tidal range of 0.35 m which is consistent with tidal ranges on intertidal mudflats which can range from 0.1 m to 1 m depending on the location [21,24]. No wind forcing was applied, consistent with the objective of isolating wave-induced sediment dynamics.

Spectral wave forcing was imposed at the open boundary of the

WAVE module using a constant moderate wave-exposed condition: significant wave height (H_{sig}) = 1.0 m, peak wave period (T_p) = 8.0 s, and mean wave direction (D_m) = 10°, perpendicular to the shoreline. These wave conditions were consistent with previous studies involving mangrove restoration where wave heights ranged from 1 m to 2.5 m [21, 24]. However, it is important to note that this wave condition was not intended to represent calm interior mangrove flat conditions. Rather, it was selected as a wave-exposed restoration scenario in which unassisted seedling establishment would be physically challenging and where the potential role of WECs as wave attenuating preconditioning structures could be evaluated. The imposed wave height is, therefore, interpreted as a stress test condition for the proposed hybrid restoration framework.

The WEC array was represented as a series of idealized bottom-mounted oscillating wave surge converter-type devices, similar to devices like the WaveRoller [34,57]. These devices were treated as seabed-mounted, bottom-hinged, wave attenuating structures rather than floating WECs. The objective of this representation was not to resolve device motion, power take-off dynamics, structural response, or frequency-dependent hydrodynamic behaviour, but to capture the effect of a nearshore WEC array on wave attenuation, reflection, and subsequent morphodynamic change.

In the Delft3D-WAVE/SWAN module, the WECs were represented as partially reflective and partially transmissive obstacles using prescribed reflection and transmission coefficients. The transmission coefficient K_t defines the ratio between the transmitted wave height and the incident wave height:

$$K_t = \frac{H_t}{H_i} \tag{4}$$

where H_i is the incident wave height and H_t is the transmitted wave height behind the obstacle. Similarly, the reflection coefficient K_r represents the reflected component of the incident wave field. In this study, $K_t = 0.2$ and $K_r = 0.8$ were applied to represent a strongly wave-attenuating, highly reflective bottom-mounted device. These values were selected to approximate the behaviour of rigid or bottom-hinged seabed-mounted WECs and are consistent with the range of values commonly used in previous numerical wave farm modelling studies [32, 34,57].

A linear array of 10 WECs, each 12.5 m wide, was positioned approximately parallel to the shoreline and perpendicular to the incoming wave direction as seen in Fig. 1. The devices were located at either 300 m or 500 m from the shoreline, depending on the scenario, with inter-device gap spacings of 2D, 4D, or 6D, where D is the device width.

The cohesive sediment parameters used in Delft3D were selected independently of the DESOTO grain-size data. The numerical model was designed to represent an idealized fine-grained restoration frontage where erosion reduction and substrate stability are central to mangrove establishment. Therefore, the model does not assume that the DESOTO sediment conditions and the Delft3D sediment bed are identical. Rather, the biological anchorage data and the morphodynamic model represent two linked components of a proof-of-concept framework: field-derived seedling resistance thresholds are combined with idealized modelled erosion and wave-drag conditions to evaluate relative changes in survivability among WEC scenarios.

Sediment transport was modelled using the cohesive sediment module in Delft3D-FLOW, following the Partheniades-Krone formulation. Key parameter values were selected based on recommendations from the Delft3D-FLOW User Manual and previously published papers to reflect typical coastal mud conditions. The sediment density was set to 2650 kg/m^3, and the dry bed density was set to 500 kg/m^3, consistent with consolidated estuarine mud. The critical shear stress for erosion (τ_{ce}) was specified as 0.4 N/m^2, and the erosion parameter was set to 1.0×10^{-4} kg/m^2/s, representing moderately resistant cohesive beds. The critical shear stress for sedimentation (τ_{cd}) was set to 0.05 N/m^2 to represent a conservative low-deposition threshold for fine cohesive sediment. Under this formulation, deposition is permitted only when bed shear stress falls below a very low value, meaning that sediment accumulation is restricted to genuinely low-energy zones. This value was intentionally selected to avoid forcing widespread deposition in the model domain under the imposed wave-exposed condition. As a result, the model provides a conservative test of whether WECs can reduce wave energy and erosion sufficiently to improve substrate stability, rather than assuming that WEC deployment will automatically generate sediment accretion. Settling velocities for both fresh and saline conditions were defined as 0.1 mm/s, within the typical range (0.05–0.5 mm/s) for fine-grained, flocculated sediments. Therefore, in this study, WEC-induced “preconditioning” refers primarily to wave attenuation, bed-shear-stress reduction, and erosion mitigation. It does not imply that WECs alone are sufficient to create depositional mangrove habitat without additional sediment supply or elevation-building interventions. These values were consistent with cohesive sediment modelling in previous studies [46,48,56]. Bed evolution was calculated using the Exner equation, and sediment transport processes were fully coupled with the FLOW and WAVE modules.

The coupled model was run from 1 January 2025 to 31 January 2025 with a time step of 1 min. A MORFAC of 10 was applied to extrapolate morphodynamic changes over a longer period, equivalent to approximately 10 months of morphodynamic evolution. The model was first run without WECs to establish baseline wave and morphodynamic conditions and the model was then run with the WEC array. This value was selected as a moderate acceleration factor to capture cumulative erosion and sediment-retention patterns over a preconditioning period while avoiding the use of a very large acceleration factor that could distort short-term hydro-morphodynamic feedbacks. The same MORFAC value was applied consistently across all baseline and WEC scenarios, so the analysis focuses on relative differences among WEC configurations rather than absolute long-term morphological prediction.

The 10-month equivalent period was selected to represent an initial WEC-assisted site-preconditioning phase before potential mangrove planting. This timescale is long enough to evaluate whether WEC-induced wave attenuation can reduce erosion and improve bed stability over a restoration-relevant preparation period, but short enough to avoid implying multi-year or decadal prediction under constant wave forcing and idealized sediment supply. Therefore, the model results should be interpreted as comparative indicators of short-to medium-term hydrodynamic and erosional preconditioning, rather than as a fully calibrated long-term morphodynamic forecast.

2.3.3. Model scenarios and sensitivity testing

To assess sensitivity to WEC array configuration, a total of six wave farm scenarios were tested by varying both the distance from shore and the spacing between devices. Two distances were evaluated: 300 m and 500 m from the shoreline. For each distance, three inter-device gap spacings were tested: 2D (25 m), 4D (50 m), and 6D (75 m), where D is the width of a single WEC. These configurations were compared against a control scenario without WECs. All scenarios were forced with fixed wave conditions representative of moderate swell (1 m significant wave height, 8 s peak period), and sediment was modelled as cohesive mud. The simulations were analyzed to evaluate wave height attenuation, sediment transport patterns, and implications for mangrove root stability and survivability under different WEC array layouts. A summary of the model scenarios is presented in Table 2.

To evaluate the hydro-morphodynamic performance of each WEC configuration, wave attenuation, erosion reduction, sediment volume retained, and sediment retention per unit area were calculated using the same area-based comparative approach applied in Boodoo et al. [32,34]. Each WEC scenario was compared against the no-WEC control case over the corresponding evaluation area.

Wave height attenuation was calculated point-by-point by comparing the significant wave height in each WEC scenario with the

Table 2
Summary of model scenarios used for sensitivity testing.

Scenario ID	Description	Wave Conditions (Hsig, Tp)	WEC Position (m offshore)	Gap Spacing
C	Control (no WECs)	1 m, 8 s	—	—
H	Hybrid – Base Case	1 m, 8 s	500 m	2D (25 m)
D1	WECs closer to shore	1 m, 8 s	300 m	2D (25 m)
G1	Wider spacing (4D)	1 m, 8 s	500 m	4D (50 m)
G2	Widest spacing (6D)	1 m, 8 s	500 m	6D (75 m)
D1-G1	300 m offshore with wider spacing (4D)	1 m, 8 s	300 m	4D (50 m)
D1-G2	300 m offshore with widest spacing (6D)	1 m, 8 s	300 m	6D (75 m)

corresponding no-WEC control condition:

$$A_{H,i} = \left(\frac{H_{sig,noWEC,i} - H_{sig,WEC,i}}{H_{sig,noWEC,i}} \right) \times 100 \tag{5}$$

where $A_{H,i}$ is the wave height attenuation (%) at grid cell i, $H_{sig,noWEC,i}$ is the significant wave height at grid cell i in the no-WEC control scenario, and $H_{sig,WEC,i}$ is the significant wave height at the same grid cell in the WEC scenario. The wave attenuation values reported in Table 4 represent the spatially averaged attenuation over the evaluation area.

The total sediment volume retained due to the WEC array was calculated from the difference in cumulative bed level change between the WEC and no-WEC scenarios:

$$V_{sediment} = \sum_{i=1}^{N} \left(E_{WEC,i} - E_{noWEC,i} \right) \cdot A_{cell} \tag{6}$$

where $E_{WEC,i}$ and $E_{noWEC,i}$ are the cumulative erosion or accretion values at grid cell i for the WEC and no-WEC scenarios, respectively, A_{cell} is the area of a single grid cell, and N is the number of grid cells within the evaluation area. A positive value of $V_{sediment}$ indicates reduced net erosion or increased sediment retention due to the WEC array.

The percentage erosion reduction was calculated as:

$$\eta = \frac{V_{sediment}}{|V_{noWEC}|} \times 100 \tag{7}$$

where the baseline sediment volume is:

$$V_{noWEC} = \sum_{i=1}^{N} E_{noWEC,i} \cdot A_{cell} \tag{8}$$

Taking the absolute value of V_{noWEC} ensures consistency when the control area experiences net erosion. Finally, sediment retention per unit area was calculated as:

$$R = \frac{V_{sediment}}{A_{zone}} \tag{9}$$

where:

$$A_{zone} = N \cdot A_{cell} \tag{10}$$

Here, R is the sediment retention per unit area $\left(m^3 / m^2\right)$, and A_{zone} is the total evaluation area. This metric normalizes sediment retention by spatial extent and enables comparison among WEC configurations with different array footprints.

2.4. Erosion-adjusted anchorage and spatial suitability mapping

Previous studies have shown that Type I uprooting where wave-induced drag forces alone exceed the anchorage resistance of seedling roots, is highly unlikely to occur under typical flow conditions. Instead, Type II uprooting, caused by progressive substrate erosion around the roots, is the dominant mechanism of seedling failure in field environments [58–60] (Fig. 2). Kibler et al. [18] concluded that Type I failure is unlikely under natural conditions, as critical flow velocities required to overcome anchorage (1.2–1.5 m/s) are rarely reached. Instead, Type II failure where sediment erosion undermines root stability is the dominant mode of failure for young seedlings in the field.

Accordingly, this study prioritizes Type II failure but does not model Type I as a separate mechanism. Zones were only considered suitable if (i) cumulative erosion remained below the morphology-specific rooting depth, and (ii) the wave-induced drag force did not exceed the adjusted anchorage strength (Equation (12)). In cases where no erosion occurred, the full anchorage was preserved. This approach ensures that survivability is always evaluated through a Type II lens, where root destabilization due to erosion is the prerequisite for failure.

It is important to note that water depth was not used as an exclusion criterion in the suitability analysis. Although the areas are deeper than the intertidal elevation typically required for mangrove colonization, these areas are interpreted as hydrodynamically preconditioned zones where wave energy has been sufficiently reduced by the WECs. It was assumed that site preparation interventions such as mud nourishment or raised sediment platforms could be used to elevate the bed into a suitable planting range, consistent with real-world sedimentation-enhancing strategies [44].

To assess mangrove seedling survivability under different wave energy conditions, an erosion-adjusted anchorage framework was developed that integrates field-derived resistance thresholds with modelled seabed erosion from Delft3D.

For each morphology group defined in Section 2.2 two key parameters were extracted: mean anchorage, F_R from field uprooting tests and mean rooting depth, z_0 estimated from the median longest root length of corresponding groups in the lab dataset. Wave-induced erosion from Delft3D was computed as the change in bed level elevation over the simulation period:

$$\Delta z_b = z_{b\text{-final}} - z_{b\text{-initial}} \tag{11}$$

where Δz is negative when erosion occurs. Anchorage resistance at each grid cell was then dynamically adjusted based on the proportion of root zone lost to reduce anchorage resistance with erosion at the location and increase anchorage resistance as accretion occurred.

$$F_R^{\text{adjusted}} = F_R \cdot \left(1 + \frac{\Delta z}{z_0} \right) \tag{12}$$

If erosion depth exceeded the rooting depth, the adjusted resistance was set to zero. This approach assumes that anchorage decreases with erosion until complete uprooting occurs. At each grid cell in the Delft3D model domain, the wave-induced drag force acting on a mangrove seedling was calculated using the standard drag force equation:

$$F_D = \frac{1}{2} \rho C_D A_f u^2 \tag{13}$$

where F_D is the wave-induced drag force acting on the seedling shoot (N), ρ is the water density (kg/m^3), C_d is the drag coefficient, A_f is the measured shoot frontal area (m^2), and u is the representative wave orbital velocity (m/s). The frontal area A_f was obtained directly from the Kibler et al. [18] dataset and represents the projected shoot area of each seedling morphology group. Therefore, the calculated drag force was interpreted as a bulk estimate of the wave-induced force acting on the whole seedling shoot, rather than as a force acting only at the bed.

The orbital velocity u was extracted directly from the Delft3D-WAVE

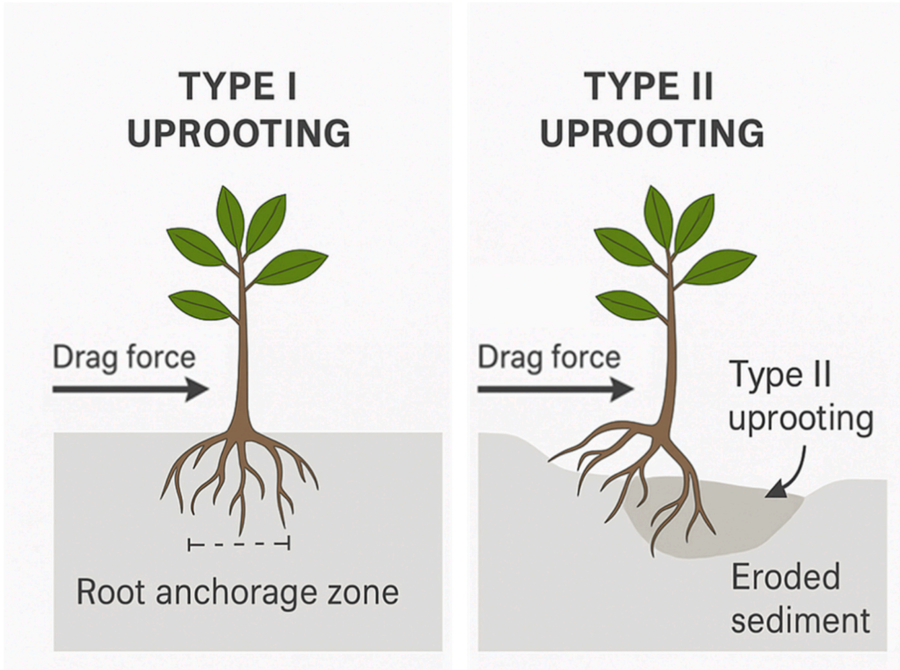

Fig. 2. Conceptual diagram of Type I and Type II uprooting.

output as the near-bed wave orbital velocity. In the present framework, this value was used as a representative bulk velocity over the exposed seedling frontal area. This assumption was adopted because the Delft3D model does not resolve plant-scale vertical velocity gradients and because the objective of this study was to develop a first-order spatial survivability framework rather than a fully resolved vegetation-force model. The use of near-bed orbital velocity is also consistent with the erosion-adjusted anchorage framework adopted here, where seedling failure is controlled by the combined effects of wave-induced drag and erosion-driven reduction in root anchorage.

A constant drag coefficient of $C_d = 1.0$ was used for all morphology groups. This value was selected as a first-order bulk drag coefficient for seedling-scale vegetation drag and is consistent with commonly used values for cylinder-like vegetation elements and field-derived estimates for mangrove vegetation. For example, Yoshikai et al. [61] reported a field-derived drag coefficient of approximately $C_d = 1.0 \pm 0.2$ for a planted *Rhizophora* mangrove forest, while other mangrove and vegetation studies show that C_d can vary depending on Reynolds number, vegetation geometry, flexibility, submergence, and wave conditions. Therefore, the calculated drag forces should be interpreted as first-order estimates, and future site-specific applications should include sensitivity testing or calibration of C_d using species-specific flume or field measurements. This approach does not explicitly resolve the vertical distribution of hydrodynamic force along the seedling height. Instead, it treats the measured shoot frontal area and representative orbital velocity as a bulk force approximation suitable for comparing relative survivability among WEC scenarios.

A binary classification was applied at each grid cell for each morphology group. Cells were labelled as.

i Suitable if $F_D < F_R^{adjusted}$
ii. Unsuitable if $F_D > F_R^{adjusted}$

Suitability maps were generated for all morphology groups (small, medium, large) and all hydrodynamic scenarios (with and without WECs, and under different wave energy conditions). To evaluate seedling survivability, each grid cell was assigned a suitability class based on the outcome of the survivability analysis and the morphological group that could persist under the simulated conditions. Suitability was categorized into four classes.

i. Class 0 = Unsuitable (none of the morphology groups can survive),
ii. Class 1 = Suitable for Small + morphologies (Groups 0, 1, and 2 can survive),
iii. Class 2 = Suitable for Medium + morphologies (Groups 1 and 2 can survive),
iv. Class 3 = Suitable for Large only (only Group 2 can survive).

The change in total suitable area was quantified across scenarios to assess the protective benefit of wave energy converters in expanding survivable zones for mangrove planting.

3. Results

3.1. Morphology grouping and anchorage resistance

Kibler et al. [18] conducted field and laboratory experiments to quantify mangrove seedling anchorage and identify the morphological traits that influence resistance to uprooting. Using a combination of shoot and root characteristics including shoot height, stem diameter, root length, and both aboveground and belowground biomass, generalized linear models (GLMs) were developed to predict pull-out force. The best-fit models yielded R^2 values of 0.5645 for field data and 0.8461 for laboratory data, indicating predictive power, particularly under controlled conditions. The study found that pull-out force increased with seedling size, ranging from as low as 10 N in smaller individuals to over 80 N in more mature seedlings. These findings highlighted the value of morphological traits, particularly AGB and BGB as predictors of anchorage performance.

Building on these findings, this study applied a process-based classification approach to group seedlings into three morphology classes: small, medium, and large using K-means clustering of AGB and BGB. These two traits were selected as functional indicators of developmental maturity and anchorage potential. AGB represents shoot development and potential drag exposure, while BGB reflects root system investment and resistance to uprooting. The clustering results (Fig. 3) showed clear separation among groups in trait space. Group 0 represented the smallest seedlings with the lowest biomass, Group 1 comprised intermediate-sized individuals, and Group 2 included the most mature seedlings with the highest AGB and BGB values. This stratification provides a biologically meaningful basis for assessing survivability potential under varying erosion and wave exposure conditions.

The distribution of pull-out forces across groups (Fig. 4) showed clear and consistent differences. Group 0 seedlings exhibited low anchorage resistance with a relatively narrow interquartile range, suggesting uniformly weak rooting. Group 1 showed both increased median resistance and a broader spread, indicating greater variability in intermediate seedlings. Group 2 had the highest median pull-out force and the widest range of values, with some individuals exceeding 80 N, reflecting both strong root development and greater heterogeneity among mature seedlings. These patterns demonstrate that biomass-based morphological groups not only reflect growth stage but also translate directly into functional differences in anchorage capacity, which are critical for survivability under erosive wave conditions.

To parameterize the survivability model, each morphology group was assigned a mean rooting depth and shoot frontal area using data from the corresponding lab dataset. Rooting depths were estimated as 8.6 cm for Group 0, 10.4 cm for Group 1, and 12.3 cm for Group 2, while frontal areas were 1505.6 mm^2, 2393.1 mm^2, and 2920.5 mm^2, respectively (Table 3). These parameters were used in the erosion-adjusted anchorage model and wave drag force equation to determine thresholds for uprooting under different hydrodynamic scenarios.

3.2. Wave attenuation and morphodynamic changes

Wave attenuation, associated morphodynamic changes, and theoretical wave energy production were assessed across all scenarios (Table 4) to evaluate the performance of various WEC configurations in simultaneously reducing nearshore hydrodynamic forcing, mitigating sediment loss, and producing renewable energy. The control scenario (C), without WECs, served as a baseline against which all other configurations were compared. Key metrics evaluated include wave height attenuation, erosion reduction, sediment volume retained, sediment retention per unit area, and theoretical wave energy output derived from Delft3D model results.

Under control conditions, wave energy reached the shoreline unimpeded (Fig. 5A), resulting in widespread erosion across the nearshore zone ranging from 0.3 m to 0.5 m (Fig. 6A). Introducing a WEC array at 500 m offshore with 2D spacing (scenario H) led to a 32.5% reduction in wave height (Fig. 5B), a 72.4% reduction in erosion, and 27,048 m^3 of sediment retained (Fig. 6B) compared to the control scenario (Fig. 5A). This configuration also yielded a total theoretical wave power output of 477 kWh for the array of 10 WECs. However, it must be noted that this represents the total theoretical power output, and the actual energy production would depend on the device efficiency and device power matrix. This scenario served as the reference for evaluating trade-offs in performance. Additionally, Fig. 6 presents cumulative bed level change from the morphodynamic model. Although this output can represent both erosion and deposition, the simulated scenarios did not produce positive deposition values, so the maps are interpreted as erosion-dominated bed-level change.

When the array was moved closer to shore (300 m) in scenario D1, wave attenuation dropped slightly (29.7%) (Fig. 5C), and erosion reduction decreased to 49.3%, with 24,209 m^3 of sediment retained (Fig. 6C). Importantly, total theoretical wave power decreased to 446.25 kWh/m, reflecting the reduced wave power available at shallower depths. Similar energy penalties were observed in the other nearshore configurations (D1-G1 and D1-G2), reinforcing the energy–protection trade-off.

Scenario G1 (4D spacing at 500 m) achieved a 69.2% erosion reduction and 30,567 m^3 of sediment retention (Fig. 6D) with 477 kWh/m of wave energy, maintaining high energy yield while improving sediment protection. G2 (6D spacing at 500 m) resulted in the highest sediment retention (Fig. 6E) (32,623 m^3) but the lowest wave attenuation (21.4%) (Fig. 5E), again with 477 kWh/m of energy, highlighting a case where spacing enhances morphodynamic benefits without reducing energy yield.

In contrast, combined configurations (D1-G1 and D1-G2) had reduced performance across all metrics. D1-G1 produced 39.9% erosion reduction, 23,290 m^3 retained, and only 446.25 kWh/m in energy. D1-G2 had the weakest overall results: 32.7% erosion reduction, 24,013 m^3

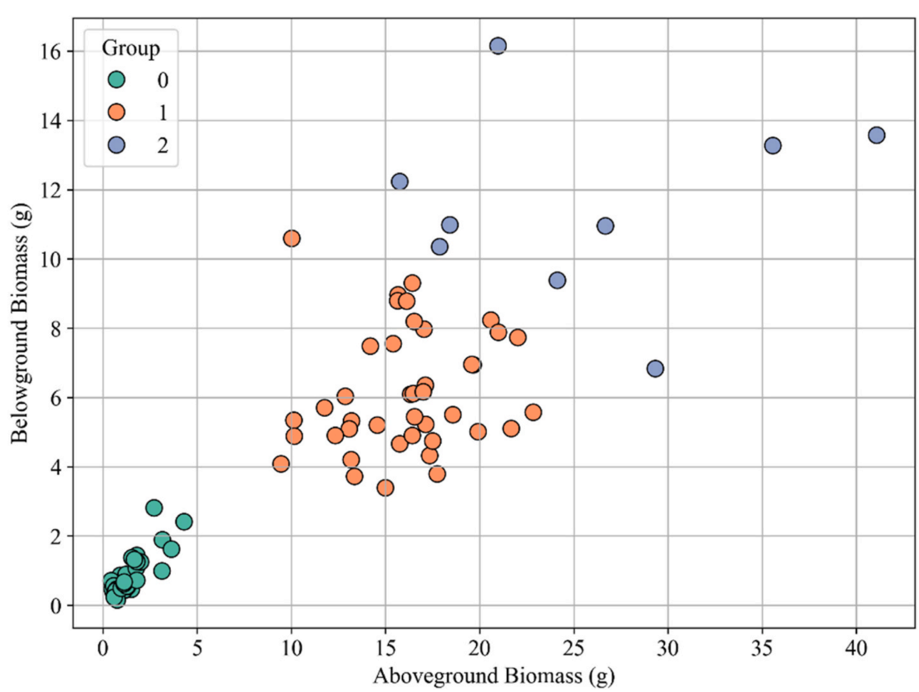

Fig. 3. K-means clustering of seedlings by AGB and BGB.

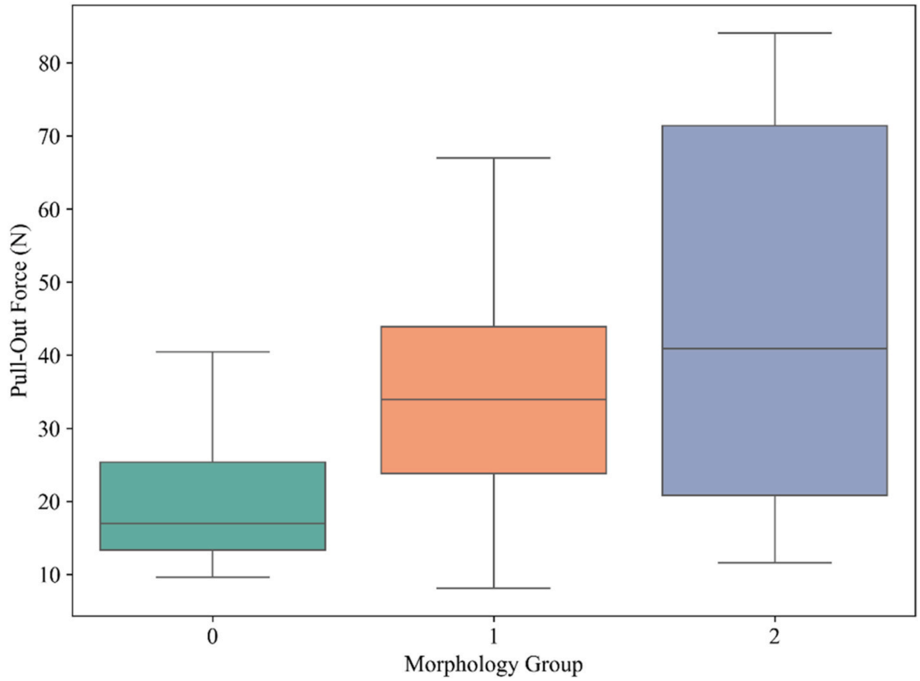

Fig. 4. Pull-out force distribution by seedling morphology group.

Table 3
Seedling morphological traits, anchorage resistance, mean frontal area and rooting depth per group.

Morphology Group	Mean AGB (g)	Mean BGB (g)	Mean Pull-Out Force (N)	Mean Root Length (cm)	Mean Frontal Area (mm^2)
0	1.43	0.83	19.7	8.8	1353.57
1	16.04	6.15	34.07	8.31	2549.69
2	25.54	11.52	43.81	11.5	4039.97

Table 4
Summary of wave attenuation, erosion reduction, sediment retention, and theoretical wave energy output for all wave farm scenarios.

Scenario	Wave height Attenuation (%)	Erosion Reduction (%)	Volume Retained (m^3)	Retention per Area (m^3/m^2)	Theoretical Energy Output (kWh/m)
H	32.5	72.4	27,048.44	0.27	477
D1	29.7	49.3	24,208.5	0.242	446.25
G1	26.6	69.2	30,566.9	0.257	477
G2	21.4	58.8	32,622.7	0.217	477
D1-G1	24.1	39.9	23,290.1	0.196	446.25
D1-G2	19.6	32.7	24,013.1	0.160	446.25

retention, and 446.25 kWh/m. These patterns illustrate how trade-offs between wave attenuation, erosion mitigation, and energy output depend strongly on device spacing and placement relative to both bathymetry and prevailing wave energy.

Although the WEC arrays substantially reduced erosion behind the device zones, no net deposition was observed in any scenario. This result is important because it shows that WEC-induced wave attenuation alone was not sufficient to trigger cohesive sediment accumulation under the imposed wave-exposed forcing and conservative sedimentation threshold. Instead, the main morphodynamic effect of the WEC arrays was erosion mitigation. Under the simulated conditions, bed shear stress frequently remained above the critical threshold for sedimentation ($\tau_{cd} = 0.05$ N/m^2), thereby limiting the potential for fine-sediment deposition.

Consequently, the results should be interpreted as demonstrating hydrodynamic and erosional preconditioning, rather than direct habitat creation. In practical restoration settings, the WEC-induced calm zones identified here would likely need to be combined with sediment-enhancing interventions, such as mud nourishment or raised planting platforms, to achieve the bed elevations and substrate conditions required for mangrove establishment.

This erosion-dominated behaviour is particularly relevant in the context of mangrove anchorage. As described in the following section, suitability for seedling establishment was evaluated using an erosion-adjusted anchorage model. Even without net sedimentation, local reductions in erosion within the WEC-induced calm zones contributed meaningfully to improving anchorage conditions and seedling stability. However, the absence of sediment accumulation also highlights the need for additional site preparation (e.g., elevation gains through mud nourishment or engineered platforms) if mangrove planting is to be viable in these deeper zones.

WECs demonstrated the potential to simultaneously reduce wave energy, limit erosion, and generate renewable energy. Among the tested configurations, Scenario H achieved the highest erosion reduction and retention efficiency, while Scenario G1 offered a strong balance between sediment protection and maximum energy output. Although Scenario G2 retained the greatest total sediment volume, its retention efficiency and wave attenuation were comparatively lower. These results illustrate the inherent trade-offs between nearshore protection and offshore energy optimization, emphasizing the need to evaluate configurations based on the specific performance priorities of a given project. The wave height maps shown in Fig. 5 represent the final Delft3D-WAVE output at the end of the coupled simulation period, after the morphodynamic bed update associated with the 10-month equivalent simulation period.

3.3. Spatial habitat suitability

Habitat suitability for mangrove restoration was assessed for each WEC scenario by comparing hydrodynamic drag forces with the anchorage resistance of three mangrove morphological groups. Suitability was categorized into four classes: 0 = unsuitable, 1 = suitable for

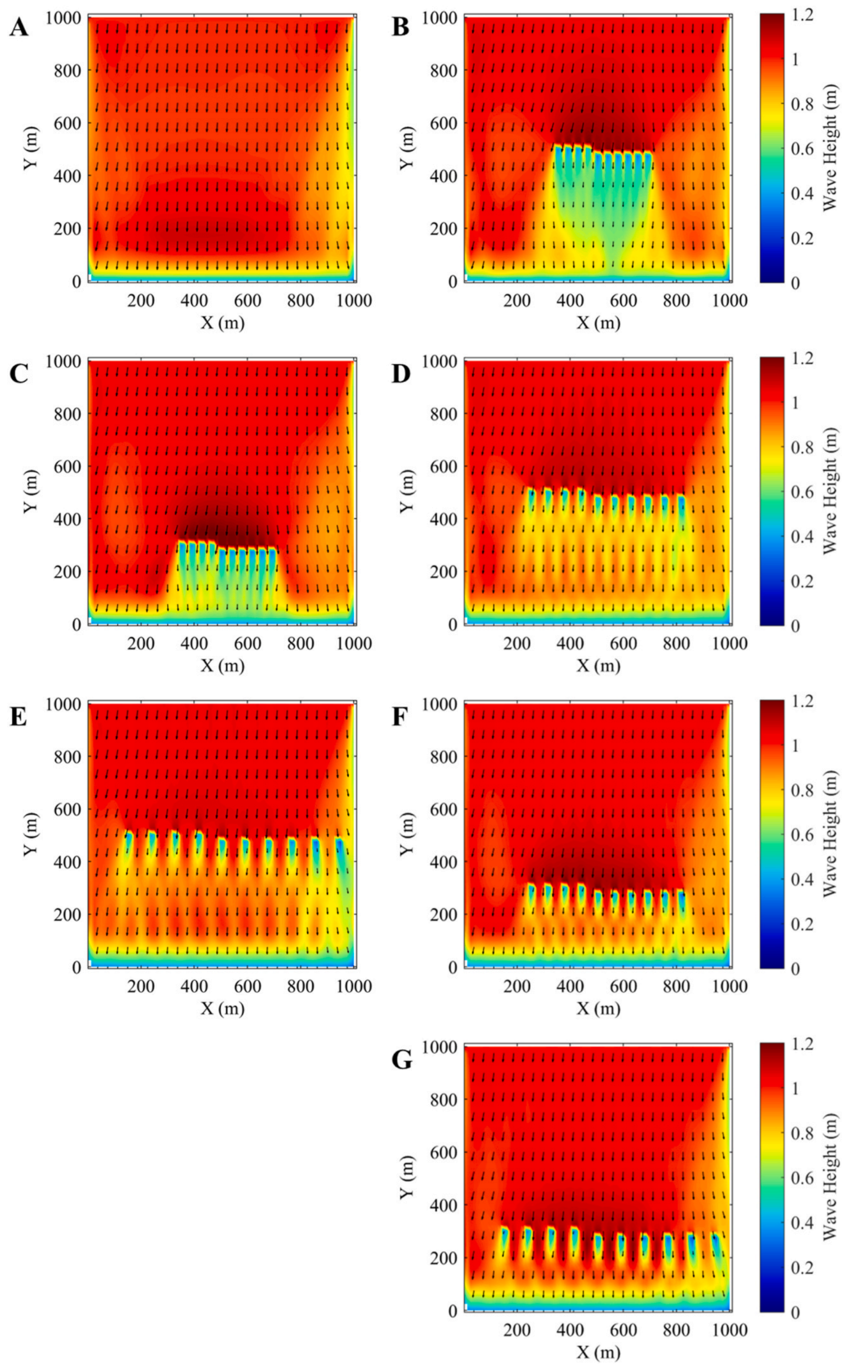

Fig. 5. Spatial distribution of significant wave height (H_{sig}) at the final model output time for all scenarios: (A) Control, (B) Base, (C) D1, (D) G1, (E) G2, (F) D1-G1, and (G) D1-G2.

small + morphologies, 2 = medium+, and 3 = large only (Fig. 7). Across all scenarios tested in this study, no cells met the threshold for Class 2 (medium+), likely due to the narrow margin between hydrodynamic drag and the anchorage resistance for that group. Consequently, the restoration potential was assessed based on the total area covered by Class 1 and Class 3 zones (Table 5). Class 0 areas were omitted from Table 5 because they represent unsuitable zones and do not contribute to restoration potential. The table therefore reports only Classes 1-3, where at least one seedling morphology group satisfies the survivability criteria.

Scenario G2 yielded the largest total restoration area (90,781 m^2), comprising 62,344 m^2 suitable for small + seedlings and 28,438 m^2 suitable only for large morphologies. However, this expanded area was primarily due to the broader footprint of the 6D-spaced array, which dispersed wave energy over a larger area of the domain. Visual inspection of the habitat suitability map for G2 (Fig. 7D) revealed that this area was highly fragmented, forming disconnected patches behind individual WECs.

In contrast, the base scenario (H) produced a smaller but more spatially suitable zone (34,688 m^2), with a continuous wave shadow extending landward of the WEC array. Such a consolidated zone is likely more practical for large-scale mangrove planting, where proximity, accessibility, and root interlocking are essential for stabilization and long-term growth. The D1-G2 and G1 scenarios also performed well, offering 45,156 m^2 and 37,969 m^2 of suitable area, respectively. Conversely, scenario D1, which positioned the WEC array nearest to

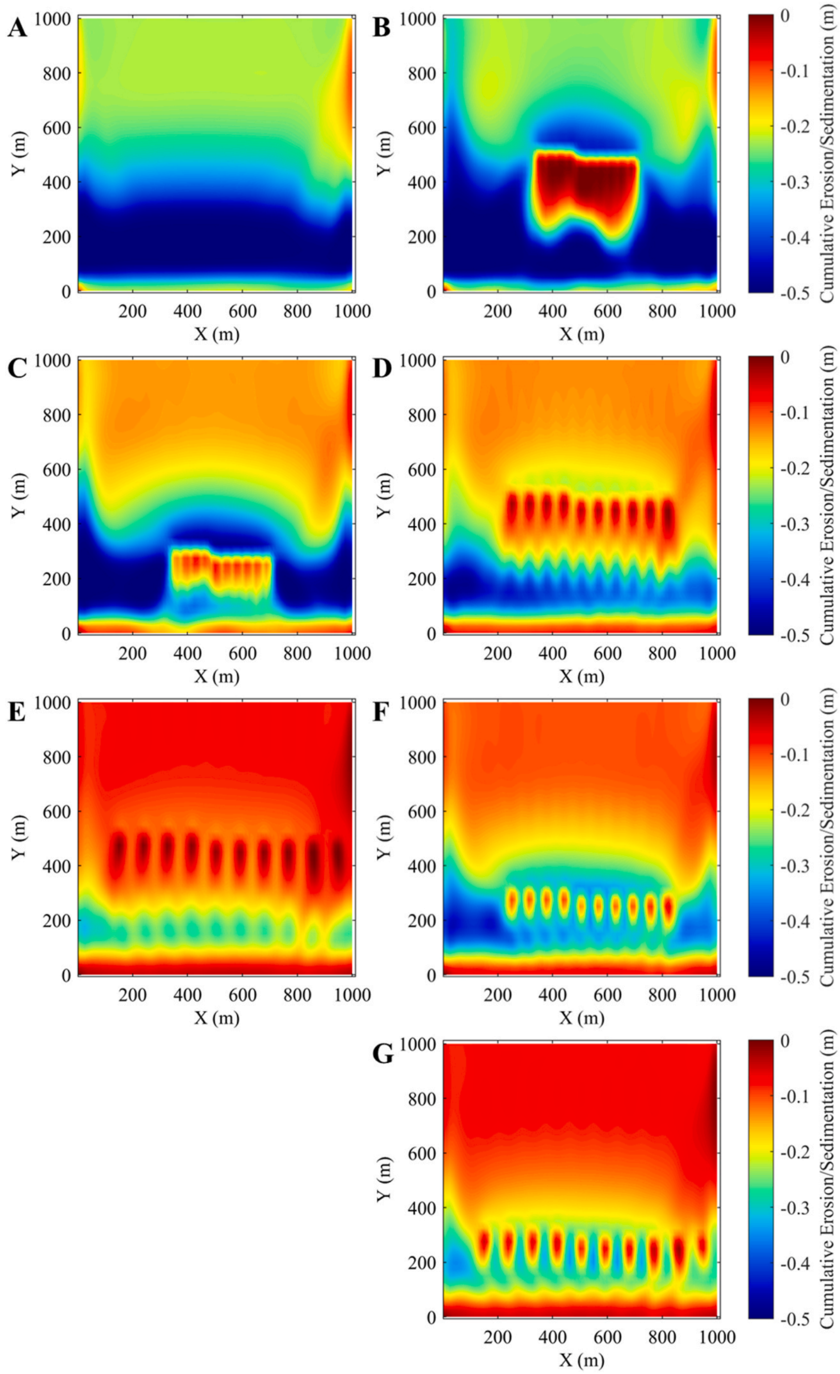

Fig. 6. Cumulative bed-level change at the final model output time for all scenarios: (A) Control, (B) Base, (C) D1, (D) G1, (E) G2, (F) D1-G1, and (G) D1-G2. Negative values indicate erosion, while values close to zero indicate limited bed-level change. Although the model output represents erosion–deposition change, no positive deposition was observed in the simulated scenarios; therefore, the maps are erosion-dominated.

shore, had the smallest restoration area (11,875 m^2), despite generating high local wave attenuation. This suggests that excessive turbulence and narrow shadow zones reduce the spatial extent of viable planting areas.

To explore trade-offs between energy production, sediment retention efficiency, and restoration potential, a 3D Pareto plot was generated (Fig. 8). Scenario G2 achieved the largest restoration area but had lower sediment retention, while Scenario H had the highest retention efficiency with a smaller but more consolidated suitability zone. Scenario G1 provided a strong balance between energy output and sediment retention. The plot underscores the importance of evaluating WEC performance through a multi-objective lens, particularly when optimizing for both ecological and engineering outcomes.

While the suitability classification was based on hydrodynamic thresholds, the actual bathymetric depths in the suitable areas ranged from 2 to 4 m, which is well below the intertidal elevations typically required for mangrove colonization. Mangroves are adapted to dynamic intertidal environments where they experience regular but partial tidal inundation. Thus, the zones identified in this study should be interpreted as hydrodynamically preconditioned areas, not necessarily ready for direct planting.

To enable successful restoration at these depths, additional elevation-building interventions would be required. This may include mud nourishment, river sediment diversions [44], or raised platforms [62] that bring the substrate into a suitable elevation range for

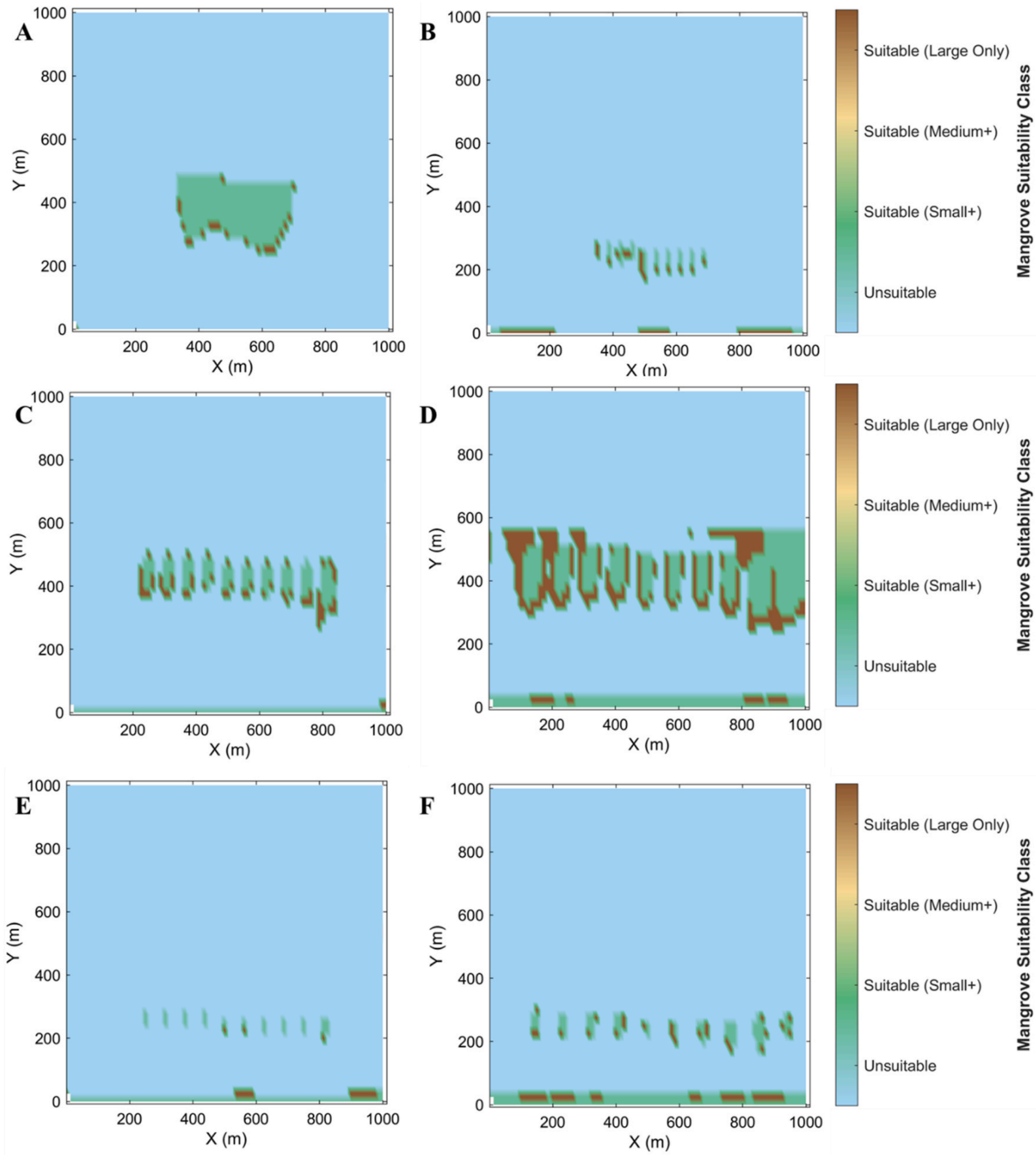

Fig. 7. Habitat suitability maps for mangrove restoration under each scenario: (A) Base (H), (B) D1, (C) G1, (D) G2, (E) D1–G1, (F) D1–G2.

Table 5
Restoration-suitable area by habitat suitability class for each WEC scenario. Class 0, representing unsuitable area, is not included because the table focuses only on restoration-relevant suitable zones. Total restoration area includes Classes 1–3 only.

Scenario	Class 1 Area (m^2)	Class 2 Area (m^2)	Class 3 Area (m^2)	Total Restoration Area (m^2)
Base (H)	31250	0	3437.5	34687.5
D1	3906.25	0	7968.75	11875
G1	28906.25	0	9062.5	37968.75
G2	62343.75	0	28437.5	90781.25
D1-G1	15781.25	0	3125	18906.25
D1-G2	29375	0	15781.25	45156.25

mangrove root establishment.

4. Discussion

4.1. *Performance trade-offs across WEC configurations*

The results demonstrate that WEC configuration plays a critical role in shaping the balance between energy production and ecological restoration potential. Importantly, the differences observed between scenarios were not just quantitative but also spatial, affecting the shape, connectivity, and practicality of potential restoration zones.

The strong performance of Scenario H in erosion reduction and retention efficiency suggests that tighter, more consolidated arrays may be more effective at creating concentrated zones of lower wave energy. This, in turn, supports sediment stabilization and the formation of areas suitable for restoration. However, the reduced spatial footprint highlights a trade-off; these configurations may fail to influence a broader area or generate expansive restoration zones, especially in deeper offshore locations.

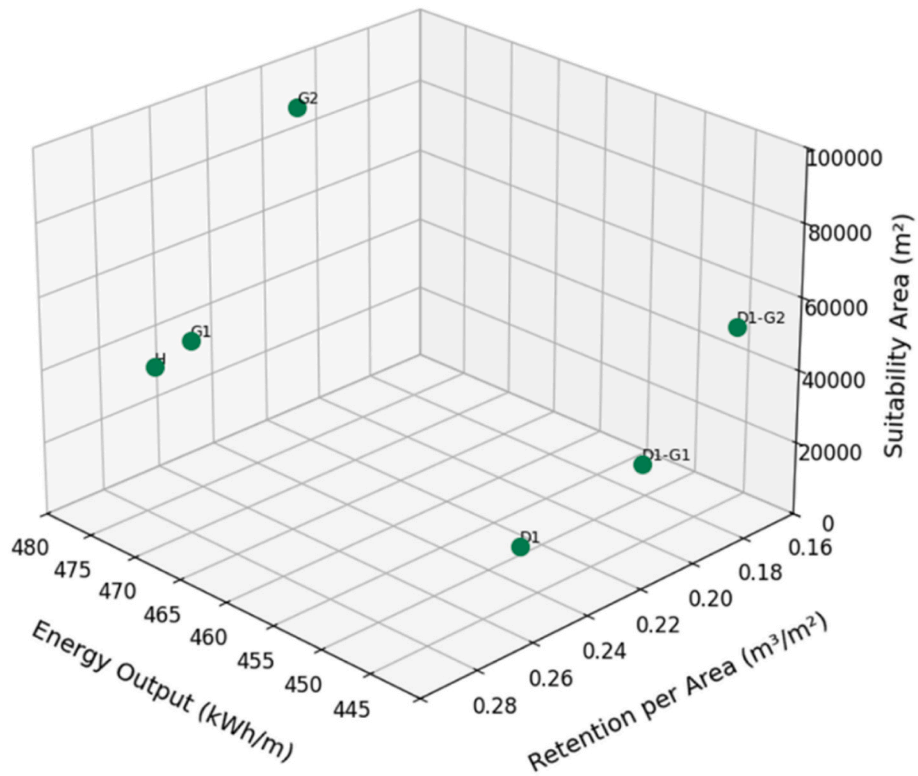

Fig. 8. 3D Pareto plot showing trade-offs between energy output, retention efficiency, and restoration area across WEC scenarios.

In contrast, the broader restoration zones observed in more widely spaced configurations (e.g., G2) suggest that increasing inter-device distance enables wave energy to dissipate over a larger area, preconditioning wider regions of the domain. Yet, the reduced energy dissipation and the fragmented nature of suitability zones imply that these layouts may be less efficient in terms of ecological or logistical restoration outcomes. Fragmented zones may hinder mangrove seedling connectivity, increase vulnerability to edge effects, and complicate restoration logistics such as planting access and maintenance.

While theoretical energy output remained constant for most scenarios (e.g., 477 kWh/m in H, G1, and G2), the actual recoverable energy in real-world settings depends on local wave conditions and the specific power matrix of the WEC device. In this study, the maximum theoretical wave power was calculated. In practice, variations in incident wave energy, device efficiency, and load hours can affect yield.

Ultimately, the choice of WEC configuration should reflect project priorities and site-specific conditions. Factors such as wave energy potential, sediment type, bathymetry, and restoration goals will influence the optimal design. This study, while based on simplified and idealized conditions, serves as a proof-of-concept demonstrating a novel methodology for assessing the trade-offs involved in hybrid WEC deployment. The framework developed here can be applied to real-world sites, allowing decision-makers to explore configuration options aligned with local environmental and socioeconomic priorities.

4.2. Role of WECs in preconditioning sites for mangrove restoration

While the habitat suitability maps identified zones of reduced wave force and erosion, particularly in the sheltered wake of WEC arrays, these areas were typically located in water depths of 2 to 4 m. Such depths fall well below the intertidal elevation range typically required for natural mangrove colonization. Mangroves rely on regular, partial tidal inundation for seedling establishment, oxygen exchange, and nutrient cycling. Therefore, although these zones were hydrodynamically favourable in terms of survivability, they are not immediately viable for planting without further intervention.

This finding highlights the potential role of WECs as site preconditioning tools rather than standalone restoration solutions. By attenuating wave energy and reducing bed shear stress, WECs create low-energy zones that could enable sediment accumulation and support future mangrove establishment. However, to transform these zones into plantable areas, elevation-building interventions would be essential. Such interventions may include mud nourishment, sediment diversions, or the use of engineered platforms or terraces to raise the seabed into the intertidal zone.

Importantly, the habitat suitability classification used in this study was based solely on hydrodynamic thresholds for erosion and drag. While these thresholds reflect critical survivability limits for uprooting, they do not capture the full range of physical requirements for mangrove establishment, most notably, elevation and soil development. As such, the suitability maps should be interpreted as identifying preconditioned zones, rather than ready-to-plant areas. Translating these zones into functioning ecosystems would require integration with engineered elevation strategies and long-term sediment management.

4.3. Socioeconomic Co-benefits and implementation potential

Beyond their environmental functions, hybrid WEC-based systems offer important opportunities for socioeconomic development in coastal regions [36]. By integrating wave energy extraction, shoreline protection, and ecological restoration, these systems can serve as multi-functional infrastructure that addresses both climate adaptation and local development needs.

One of the key benefits of such systems is their potential to create green employment. The installation and maintenance of WEC arrays, along with sediment management and mangrove restoration activities, can generate jobs for local communities, particularly in areas with limited economic opportunities. These activities may include skilled and unskilled labour such as WEC deployment, ecological monitoring, seedling propagation and planting, sediment replenishment, and long-term site maintenance. When supported by local training programs, such efforts could foster community stewardship and promote inclusive, long-term engagement with the restoration process. Furthermore, the decentralized nature of wave energy makes it well suited to support remote or energy-poor coastal communities, especially in regions where grid access is limited or unreliable. Coupling coastal restoration with renewable energy generation may offer cost-effective, sustainable infrastructure that delivers both environmental and human benefits.

The proposed framework also has implications for blue carbon planning, although carbon sequestration was not directly quantified in this study. Mangroves are widely recognized as blue carbon ecosystems because they can store carbon in aboveground biomass, belowground biomass, and organic-rich sediments. In this context, wave farm layout optimization could provide an indirect blue carbon benefit by improving the physical conditions required for mangrove regeneration. Configurations that produce more continuous low-energy zones, reduce erosion, and support sediment stability may increase the likelihood of successful seedling establishment and long-term mangrove persistence. Therefore, WEC array design should not only be evaluated in terms of energy output and erosion reduction, but also in terms of its potential to support future ecosystem recovery and carbon-storage functions when combined with appropriate elevation-building and sediment-management interventions. However, because this study did not simulate mangrove growth, biomass accumulation, or soil carbon dynamics, the blue carbon implications should be interpreted as a potential co-benefit and an important direction for future research rather than as a quantified outcome.

Finally, the successful implementation of hybrid WEC–restoration projects will require coordination across government, industry, and local stakeholders. Industry partners can contribute technical expertise and innovation; government agencies can provide regulatory support, funding, and integration into national adaptation strategies; and local communities can supply labour, knowledge of the coastal system, and long-term stewardship. These multi-stakeholder partnerships are essential to ensure that the social, economic, and environmental benefits of such systems are fully realized.

4.4. Model limitations and future research directions

While this study presents a novel framework for evaluating the hybrid potential of WECs in coastal protection and restoration, several limitations should be acknowledged. These limitations point to important opportunities for future research and model refinement.

First, the model uses an idealized, schematized bathymetry with a uniform 1:80 slope. This simplification enabled controlled comparison of WEC configurations but does not represent the full range of natural mangrove restoration settings. In particular, many muddy mangrove coasts and intertidal flats have gentler gradients and more complex depositional platforms than the profile used here. Therefore, the 1:80 slope should be interpreted as a simplified wave-exposed transition profile rather than a universally representative muddy mangrove coast. Future studies should apply the framework to site-specific bathymetry, including lower-gradient mudflats, tidal creeks, and shallow depositional shelves where WEC-induced reductions in bed shear stress may more readily support sediment accumulation.

Second, the model was forced using a constant $H_s = 1.0$ m and $T_p = 8.0$ s wave condition. This was selected as a moderate wave-exposed stress test scenario, not as a representation of calm interior mangrove hydrodynamics. While this allowed the ability of WECs to reduce energetic wave forcing to be evaluated, it may also explain why no net deposition occurred in the simulations. Future work should include lower-energy wave climates, seasonal wave variability, and external sediment supply to determine whether WEC-induced attenuation can transition from erosion mitigation to net accretion under more favourable restoration conditions.

Third, the biological anchorage data and the numerical model represent different components of the framework. The Florida seedling dataset was used to derive morphology-specific anchorage and frontal-area thresholds, while the Delft3D domain was used as an idealized hydro-morphodynamic test environment. The results should therefore be interpreted as a transferable modelling framework rather than a site-specific prediction for the Florida study sites.

Additionally, the drag-force formulation simplifies the vertical structure of hydrodynamic loading on mangrove seedlings. In reality, wave orbital velocity varies through the water column, and the exposed frontal area of a seedling may vary with height, submergence, flexibility, and leaf arrangement. The present study used a bulk drag formulation based on measured shoot frontal area and a representative near-bed orbital velocity extracted from Delft3D-WAVE. Therefore, the calculated drag force should be interpreted as a first-order survivability proxy rather than a fully resolved plant-scale force model. Future studies should improve this component by vertically integrating drag over the exposed seedling height, incorporating plant flexibility, and calibrating or testing the sensitivity of C_d using species-specific measurements.

While hydrodynamic suitability was evaluated using thresholds for drag force and bed erosion, other important biophysical factors were not modelled. These include soil shear strength, water salinity, nutrient availability, and competition between species, all of which influence mangrove establishment but are difficult to quantify in large-scale numerical models. The use of uprooting thresholds offers a useful proxy for survivability but should be supported by field-based validation and sensitivity testing in future applications.

The anchorage thresholds used in this study were derived from field seedlings growing in organic-rich mangrove substrates with sand-sized median grain diameters, whereas the Delft3D model used an idealized cohesive sediment bed. Therefore, the absolute suitability areas should be interpreted with caution. The scenario comparisons remain useful because the same morphology-specific anchorage thresholds were applied consistently across all WEC configurations; thus, differences among scenarios primarily reflect WEC-induced changes in wave forcing, erosion, and drag. Future site-specific applications should calibrate seedling anchorage resistance using local sediment conditions, including mud content, consolidation, organic matter, root–sediment interactions, and surrounding vegetation.

A MORFAC sensitivity analysis was not performed in this proof-of-concept study. Although a moderate MORFAC value of 10 was used consistently across all scenarios to support relative comparison among WEC configurations, the absolute magnitude and spatial extent of predicted bed-level change may be sensitive to the selected acceleration factor. Future site-specific applications should test multiple MORFAC values and compare accelerated results against non-accelerated or lower-acceleration simulations to confirm that hydro-morphodynamic feedbacks are not distorted.

Finally, although the modelling framework is generalizable, the results are specific to the tested WEC type and array geometries. Broader applications will require assessment of different device designs, power matrices, and anchorage characteristics, as well as incorporation of economic cost-benefit analysis to support decision-making. Taken together, these limitations underscore the need for pilot-scale field trials to validate the viability of hybrid WEC–restoration projects. Field observations would provide data to calibrate hydrodynamic and ecological models and help refine design criteria for real-world implementation.

5. Conclusions

This study presents a novel, integrated framework for evaluating the hybrid potential of WEC arrays in coastal protection and ecological restoration. Using a coupled wave–flow–morphodynamic model, the influence of different WEC configurations on wave attenuation, erosion reduction, sediment retention, and mangrove habitat suitability was assessed. Survivability was evaluated using drag-based and erosion-based uprooting thresholds, incorporating both Type 1 and Type 2 failure mechanisms.

A key innovation of this study is the use of K-means clustering to define mangrove morphological groups based on empirical measurements of above- and below-ground biomass. This allowed for a data-driven estimation of frontal area and anchorage resistance, enabling identification of zones where hydrodynamic forces exceed seedling resistance. The resulting framework is both modular and transferable. Trait data from other field sites can be similarly clustered into functional groups and applied within this modelling structure, allowing for region-specific or species-specific adaptation. This generalizable methodology offers a practical tool for restoration planning in data-limited coastal environments by bridging empirical trait data and hydro-morphodynamic modelling.

The results revealed that WEC configuration plays a critical role in shaping both physical protection and ecological suitability. Wider, offshore arrays expanded the restoration footprint but often produced fragmented suitability zones with lower retention efficiency. More compact arrays generated cohesive low-energy zones ideal for restoration but offered less spatial coverage. These trade-offs were visualized through a 3D Pareto plot, reinforcing the need for site-specific, multi-objective optimization in WEC array design.

Although hydrodynamically favourable zones were identified, most were located in 2-4 m water depths which are below natural mangrove colonization thresholds. This highlights the role of WECs as pre-conditioning tools, which must be paired with elevation building interventions such as mud nourishment or engineered terraces to enable successful planting.

Importantly, the model results should be interpreted as evidence of hydrodynamic preconditioning through wave attenuation and erosion reduction, rather than direct creation of plantable mangrove habitat. Site-specific application would require testing under local bathymetry, wave climate, sediment supply, and elevation-building conditions.

Finally, hybrid WEC systems offer broader socioeconomic value. They support job creation through device deployment, sediment management, and monitoring, while providing renewable energy and shoreline protection. Although this study was conducted under idealized conditions, it demonstrates a transferable methodology that can guide future field-based research and support the practical implementation of hybrid energy–restoration systems.

CRediT authorship contribution statement

Avinash Boodoo: Conceptualization, Data curation, Formal analysis, Investigation, Methodology, Writing – original draft, Writing – review & editing. **Deborah Villarroel-Lamb:** Investigation, Writing – review & editing. **Jeffrey S. Cross:** Writing – review & editing.

Declaration of competing interest

The authors declare that they have no known competing financial interests or personal relationships that could have appeared to influence the work reported in this paper.

Acknowledgements

The first author would like to acknowledge the Japan Ministry of Education, Culture, Sports, Science and Technology (MEXT) for financial support through the MEXT Scholarship for graduate studies. We gratefully acknowledge the use of mangrove morphological trait data from Kibler et al. [18], which supported the classification of seedling groups and estimation of anchorage resistance in this study.

References

[1] Melissa M. Baustian, Hoonshin Jung, Harris C. Bienn, Monica Barra, Scott A. Hemmerling, Yushi Wang, Eric White, Ehab Meselhe, Engaging coastal community members about natural and nature-based solutions to assess their ecosystem function, Ecol. Eng. 143 (2020) 100015, https://doi.org/10.1016/j.ecoena.2019.100015.
[2] Wen L. Chen, Peter Muller, Robert C. Grabowski, Nicholas Dodd, Green nourishment: an innovative nature-based solution for coastal erosion, Front. Mar. Sci. 8 (2022), https://doi.org/10.3389/fmars.2021.814589, 2021.
[3] Silvia Unguendoli, Luis Germano Biolchi, Margherita Aguzzi, Umesh Pranavam Ayyappan Pillai, Jacopo Alessandri, Andrea Valentini, A modeling application of integrated nature based solutions (NBS) for coastal erosion and flooding mitigation in the Emilia-Romagna coastline (Northeast Italy), Sci. Total Environ. 867 (2023) 161357, https://doi.org/10.1016/j.scitotenv.2022.161357.
[4] James Forrester, Nicoletta Leonardi, James R. Cooper, Pavitra Kumar, Seagrass as a nature-based solution for coastal protection, Ecol. Eng. 206 (2024) 107316, https://doi.org/10.1016/j.ecoleng.2024.107316.
[5] Katie K. Arkema, Robert Griffin, Sergio Maldonado, Jessica Silver, Jenny Suckale, Anne D. Guerry, Linking social, ecological, and physical science to advance natural and nature-based protection for coastal communities, Ann. N. Y. Acad. Sci. 1399 (1) (2017) 5–26, https://doi.org/10.1111/nyas.13322.
[6] E.M. Horstman, C.M. Dohmen-Janssen, P.M.F. Narra, N.J.F. van den Berg, M. Siemerink, S.J.M.H. Hulscher, Wave attenuation in mangroves: a quantitative approach to field observations, Coast. Eng. 94 (2014) 47–62, https://doi.org/10.1016/j.coastaleng.2014.08.005.
[7] P.W.J.M. Willemsen, E.M. Horstman, B.W. Borsje, D.A. Friess, C.M. Dohmen-Janssen, Sensitivity of the sediment trapping capacity of an estuarine mangrove forest, Geomorphology 273 (2016) 189–201, https://doi.org/10.1016/j.geomorph.2016.07.038.
[8] Xiaoyan Zhou, Zhijun Dai, Wenhong Pang, Jie Wang, Chuqi Long, Wave attenuation over mangroves in the nanliu Delta, China, Front. Mar. Sci. 9 (2022), https://doi.org/10.3389/fmars.2022.874818, 2022.
[9] Ekaningrum Damastuti, Bregje K. van Wesenbeeck, Rik Leemans, Rudolf S. de Groot, Marcel J. Silvius, Effectiveness of community-based mangrove management for coastal protection: a case study from Central Java, Indonesia, Ocean Coast Manag. 238 (2023) 106498, https://doi.org/10.1016/j.ocecoaman.2023.106498.
[10] Qiang Chen, Yuepeng Li, David M. Kelly, Keqi Zhang, Brian Zachry, Jamie Rhome, Improved modeling of the role of mangroves in storm surge attenuation, Estuar. Coast Shelf Sci. 260 (2021) 107515.
[11] Maria Maza, Javier L. Lara, Inigo J. Losada, Tsunami wave interaction with mangrove forests: a 3-D numerical approach, Coast. Eng. 98 (2015) 33–54, https://doi.org/10.1016/j.coastaleng.2015.01.002.
[12] Phuoc Vo-Luong, Stanislaw Massel, Energy dissipation in non-uniform mangrove forests of arbitrary depth, J. Mar. Syst. 74 (1) (2008) 603–622, https://doi.org/10.1016/j.jmarsys.2008.05.004.
[13] Rik Gijsman, Erik M. Horstman, Daphne van der Wal, Daniel A. Friess, Andrew Swales, Kathelijne M. Wijnberg, Nature-based engineering: a review on reducing coastal flood risk with mangroves, Front. Mar. Sci. 8 (2021) 702412.
[14] Xiaoxia Zhang, Pengzhi Lin, Xinping Chen, Coastal protection by planted mangrove forest during typhoon mangkhut, J. Mar. Sci. Eng. 10 (9) (2022) 1288. https://www.mdpi.com/2077-1312/10/9/1288.
[15] Thorsten Balke, Tjeerd J. Bouma, Erik M. Horstman, Edward L. Webb, Paul LA. Erftemeijer, Peter MJ. Herman, Windows of opportunity: thresholds to mangrove seedling establishment on tidal flats, Mar. Ecol. Prog. Ser. 440 (2011) 1–9.
[16] Aji Ali Akbar, Junun Sartohadi, Tjut Sugandawaty Djohan, Ritohardoyo Su, The role of breakwaters on the rehabilitation of coastal and mangrove forests in West Kalimantan, Indonesia, Ocean Coast Manag. 138 (2017) 50–59, https://doi.org/10.1016/j.ocecoaman.2017.01.004.
[17] Sophie D. Boizard, Stephen J. Mitchell, Resistance of red mangrove (Rhizophora mangle L.) seedlings to deflection and extraction, Trees 25 (3) (2011) 371–381, https://doi.org/10.1007/s00468-010-0512-z.
[18] Kelly M. Kibler, Christian Pilato, Linda J. Walters, Melinda Donnelly, Jyotismita Taye, Hydrodynamic limitations to mangrove seedling retention in subtropical estuaries, Sustainability 14 (14) (2022) 8605.
[19] Marine Le Minor, Gerhard Bartzke, Martin Zimmer, Lucy Gillis, Véronique Helfer, Katrin Huhn, Numerical modelling of hydraulics and sediment dynamics around mangrove seedlings: implications for mangrove establishment and reforestation, Estuar. Coast Shelf Sci. 217 (2019) 81–95.
[20] Bijsterveldt van, E.J. Celine, Adolphe O. Debrot, Tjeerd J. Bouma, Moch B. Maulana, Rudhi Pribadi, Jessica Schop, Femke H. Tonneijck, Bregje K. van Wesenbeeck, To plant or not to plant: when can planting facilitate mangrove restoration? Front. Environ. Sci. 9 (2022) https://doi.org/10.3389/fenvs.2021.690011.
[21] Roslan Hashim, Babak Kamali, Noraini Mohd Tamin, Rozainah Zakaria, An integrated approach to coastal rehabilitation: mangrove restoration in sungai haji dorani, Malaysia, Estuar. Coast Shelf Sci. 86 (1) (2010) 118–124, https://doi.org/10.1016/j.ecss.2009.10.021.
[22] Tu Le Xuan, Le Manh Hung, Tran Ba Hoang, Duong Do Van, Hoang Thai Duong Vu, David Wright, Van Hieu Bui, Duong Tran Anh, Wave energy dissipation through a hollow triangle breakwater on the coastal mekong Delta, Ocean. Eng. 245 (2022) 110419, https://doi.org/10.1016/j.oceaneng.2021.110419.
[23] Qinqin Liu, Xiaojian Liu, Xiaowei Zhu, Peng Hou, Changtao Deng, Huan Gao, Qisong Wang, Can Zheng, Huiqun Guo, Experimental study on the restoration and protection of mangrove tidal ecosystems flat located in a high wave area, Estuar. Coast Shelf Sci. 323 (2025) 109386, https://doi.org/10.1016/j.ecss.2025.109386.
[24] Johan C. Winterwerp, Thorsten Albers, Edward J. Anthony, Daniel A. Friess, Gijón Mancheño Alejandra, Kene Moseley, Muhari Abdul, Sieuwnath Naipal, Joost Noordermeer, Oost Albert, Saengsupavanich Cherdvong, Silke A.J. Tas,

Femke H. Tonneijck, Wilms Tom, Van Bijsterveldt Celine, Van Eijk Pieter, Van Lavieren Els, K. Bregje, Wesenbeeck Van, Managing erosion of mangrove-mud coasts with permeable dams – lessons learned, Ecol. Eng. 158 (2020) 106078, https://doi.org/10.1016/j.ecoleng.2020.106078.
[25] T. Albers, K. Schmitt, Dyke design, floodplain restoration and mangrove co-management as parts of an area coastal protection strategy for the mud coasts of the mekong Delta, Vietnam, Wetl. Ecol. Manag. 23 (6) (2015) 991–1004, https://doi.org/10.1007/s11273-015-9441-3.
[26] Ming Peng, Jingliang Zhang, Yan Zhu, Liang Gao, Shuang Li, Xinyu Pan, Experimental study on wave attenuation and stability of ecological dike system composed of submerged breakwater, mangrove, and dike under storm surge, Appl. Ocean Res. 151 (2024) 104144, https://doi.org/10.1016/j.apor.2024.104144.
[27] K. Risheharan, J. Baumeister, M.F. Adame, Are floating mangrove breakwaters effective for wave attenuation? - a Literature Review, Ecol. Eng. 211 (2025) 107436, https://doi.org/10.1016/j.ecoleng.2024.107436.
[28] S. Astariz, G. Iglesias, The economics of wave energy: a review, Renew. Sustain. Energy Rev. 45 (2015) 397–408, https://doi.org/10.1016/j.rser.2015.01.061.
[29] Bingyong Guo, John V. Ringwood, A review of wave energy technology from a research and commercial perspective, IET Renew. Power Gener. 15 (14) (2021) 3065–3090, https://doi.org/10.1049/rpg2.12302.
[30] Nisha Kaur, K. Sudhakar, M.R. Mohamed, Erdem Cuce, Dan Barbulescu, Wireless power transfer in offshore renewable energy: a review of technologies, challenges, and future directions, Unconventional Resources 9 (2026) 100287, https://doi.org/10.1016/j.uncres.2025.100287.
[31] Mayank Kalsariya, Aanya Shah, Swara Patel, Shiv Mandlik, Rajdeep Raulji, Dev Shah, Mitul Prajapati, Manan Shah, A systematic study on geothermal energy integrated water desalination: challenges and opportunities, Unconventional Resources 8 (2025) 100226, https://doi.org/10.1016/j.uncres.2025.100226. https://www.sciencedirect.com/science/article/pii/S2666519025000925.
[32] Avinash Boodoo, Tatsuya Wakeyama, Jeffrey S. Cross, Wave farms for coastal protection: a systematic review of effectiveness, methodologies, and future directions, Ocean Coast Manag. 269 (2025) 107807, https://doi.org/10.1016/j.ocecoaman.2025.107807.
[33] Mohamed Khaleel, Yusupov Ziyodulla, Advancing sustainable energy transitions: insights on finance, policy, infrastructure, and demand-side integration, Unconventional Resources 9 (2026) 100274, https://doi.org/10.1016/j.uncres.2025.100274.
[34] Avinash Boodoo, Jeffrey S. Cross, Christopher Ridgewell, Ville Kortelainen, Matti Vuorinen, Amina Harouna-Mayer, Long-term impacts and design considerations of dual-purpose wave farms for energy generation and coastal protection, Appl. Energy 401 (2025) 126805, https://doi.org/10.1016/j.apenergy.2025.126805.
[35] J. Abanades, G. Flor-Blanco, G. Flor, G. Iglesias, Dual wave farms for energy production and coastal protection, Ocean Coast Manag. 160 (2018) 18–29, https://doi.org/10.1016/j.ocecoaman.2018.03.038.
[36] Avinash Boodoo, Jeffrey S. Cross, Christopher Ridgewell, Ville Kortelainen, Matti Vuorinen, Amina Harouna-Mayer, A techno-economic framework for dual-purpose wave farms: integrating coastal protection benefits into the levelized cost of energy assessment, Energy Convers. Manag. 349 (2026) 120887, https://doi.org/10.1016/j.enconman.2025.120887.
[37] Cristobal Rodriguez-Delgado, Rafael J. Bergillos, Gregorio Iglesias, Dual wave farms for energy production and coastal protection under sea level rise, J. Clean. Prod. 222 (2019) 364–372, https://doi.org/10.1016/j.jclepro.2019.03.058.
[38] J. Abanades, D. Greaves, G. Iglesias, Coastal defence using wave farms: the role of farm-to-coast distance, Renew. Energy 75 (2015) 572–582, https://doi.org/10.1016/j.renene.2014.10.048.
[39] Rafael J. Bergillos, Cristobal Rodriguez-Delgado, James Allen, Gregorio Iglesias, Wave energy converter configuration in dual wave farms, Ocean. Eng. 178 (2019) 204–214, https://doi.org/10.1016/j.oceaneng.2019.03.001.
[40] Y. Berrio, G. Rivillas-Ospina, G. Ruiz-Martínez, A. Arango-Manrique, C. Ricaurte, E. Mendoza, R. Silva, D. Casas, M. Bolívar, K. Díaz, Energy conversion and beach protection: numerical assessment of a dual-purpose WEC farm, Renew. Energy 219 (2023) 119555, https://doi.org/10.1016/j.renene.2023.119555.
[41] Rafael J. Bergillos, Cristobal Rodriguez-Delgado, James Allen, Gregorio Iglesias, Wave energy converter geometry for coastal flooding mitigation, Sci. Total Environ. 668 (2019) 1232–1241, https://doi.org/10.1016/j.scitotenv.2019.03.022.
[42] Cristobal Rodriguez-Delgado, Rafael J. Bergillos, Miguel Ortega-Sánchez, Gregorio Iglesias, Protection of gravel-dominated coasts through wave farms: layout and shoreline evolution, Sci. Total Environ. 636 (2018) 1541–1552, https://doi.org/10.1016/j.scitotenv.2018.04.333.
[43] Cristobal Rodriguez-Delgado, Rafael J. Bergillos, Gregorio Iglesias, Dual wave farms and coastline dynamics: the role of inter-device spacing, Sci. Total Environ. 646 (2019) 1241–1252, https://doi.org/10.1016/j.scitotenv.2018.07.110.
[44] Jana R. Cox, Mandy Paauw, Jaap H. Nienhuis, Frances E. Dunn, Eveline van der Deijl, Christopher Esposito, Marc Goichot, Jasper R.F. W. Leuven, Dirk S. van Maren, Hans Middelkoop, Safaa Naffaa, Munsur Rahman, Christian Schwarz, Eline Sieben, Annisa Triyanti, Brendan Yuill, A global synthesis of the effectiveness of sedimentation-enhancing strategies for river deltas and estuaries, Global Planet. Change 214 (2022) 103796, https://doi.org/10.1016/j.gloplacha.2022.103796.
[45] G.R. Lesser, J.A. Roelvink, J.A.T.M. van Kester, G.S. Stelling, Development and validation of a three-dimensional morphological model, Coast. Eng. 51 (8) (2004) 883–915, https://doi.org/10.1016/j.coastaleng.2004.07.014.
[46] Zixiao He, Mingen Liang, Liangwen Jia, Haoyan Dong, Kanglin Chen, Jing Liu, Yitong Lin, Jintang Ou, Long-term morphological modeling and implication for estuarine regulation of the modaomen Estuary, pearl river Delta, China, Appl. Ocean Res. 123 (2022) 103184, https://doi.org/10.1016/j.apor.2022.103184.
[47] Bing Yuan, Jian Sun, Binliang Lin, Fanyi Zhang, Long-term morphodynamics of a large estuary subject to decreasing sediment supply and sea level rise, Global Planet. Change 191 (2020) 103212, https://doi.org/10.1016/j.gloplacha.2020.103212.
[48] S.M. Besselly, U. Grueters, M. van Der Wegen, J. Reyns, J. Dijkstra, D. Roelvink, Modelling mangrove-mudflat dynamics with a coupled individual-based-hydro-morphodynamic model, Environ. Model. Software 169 (2023) 105814, https://doi.org/10.1016/j.envsoft.2023.105814.
[49] Daniel R. David, P. Rijnsdorp Dirk, Jeff E. Hansen, Ryan J. Lowe, Mark L. Buckley, Predicting coastal impacts by wave farms: a comparison of wave-averaged and wave-resolving models, Renew. Energy 183 (2022) 764–780, https://doi.org/10.1016/j.renene.2021.11.048.
[50] H. Elmilady, M. van der Wegen, D. Roelvink, A. van der Spek, Modeling the morphodynamic response of estuarine intertidal shoals to sea-level rise, J. Geophys. Res. Earth Surf. 127 (1) (2022), https://doi.org/10.1029/2021JF006152 e2021JF006152.
[51] G. Mariotti, A. Canestrelli, Long-term morphodynamics of muddy backbarrier basins: fill in or empty out? Water Resour. Res. 53 (8) (2017) 7029–7054, https://doi.org/10.1002/2017WR020461.
[52] A. Nnafie, H.E. de Swart, A. Falqués, D. Calvete, Long-Term morphodynamics of a coupled shelf-shoreline system forced by waves and tides, a model approach, J. Geophys. Res. Earth Surf. 126 (12) (2021), https://doi.org/10.1029/2021JF006315 e2021JF006315.
[53] P.W.J.M. Willemsen, B.P. Smits, B.W. Borsje, P.M.J. Herman, J.T. Dijkstra, T. J. Bouma, S.J.M.H. Hulscher, Modeling decadal salt marsh development: variability of the salt marsh edge under influence of waves and sediment availability, Water Resour. Res. 58 (1) (2022), https://doi.org/10.1029/2020WR028962 e2020WR028962.
[54] T.E. Baldock, Behnam Shabani, David P. Callaghan, Zhifang Hu, Peter J. Mumby, Two-dimensional modelling of wave dynamics and wave forces on fringing coral reefs, Coast. Eng. 155 (2020) 103594, https://doi.org/10.1016/j.coastaleng.2019.103594.
[55] R. Gijsman, E.M. Horstman, A. Swales, T. Balke, P.W.J.M. Willemsen, D. van der Wal, K.M. Wijnberg, Biophysical modeling of mangrove seedling establishment and survival across an elevation gradient with forest zones, J. Geophys. Res. Earth Surf. 129 (5) (2024), https://doi.org/10.1029/2024JF007664 e2024JF007664.
[56] Bas W. Borsje, Mindert B. de Vries, Suzanne J.M. H. Hulscher, G.J. de Boer, Modeling large-scale cohesive sediment transport affected by small-scale biological activity, Estuar. Coast Shelf Sci. 78 (3) (2008) 468–480, https://doi.org/10.1016/j.ecss.2008.01.009.
[57] Avinash Boodoo, A multi-objective optimization framework for wave farm design: balancing coastal protection and energy output, Renew. Energy Focus 58 (2026) 100831, https://doi.org/10.1016/j.ref.2026.100831.
[58] Sharon Bywater-Reyes, Andrew C. Wilcox, John C. Stella, Anne F. Lightbody, Flow and scour constraints on uprooting of pioneer woody seedlings, Water Resour. Res. 51 (11) (2015) 9190–9206, https://doi.org/10.1002/2014WR016641.
[59] G. Calvani, S. Francalanci, L. Solari, A physical model for the uprooting of flexible vegetation on river bars, J. Geophys. Res. Earth Surf. 124 (4) (2019) 1018–1034.
[60] Katharina Edmaier, Benoît Crouzy, Roland Ennos, Paolo Burlando, Paolo Perona, Influence of root characteristics and soil variables on the uprooting mechanics of Avena sativa and Medicago sativa seedlings, Earth Surf. Process. Landf. 39 (10) (2014) 1354–1364, https://doi.org/10.1002/esp.3587.
[61] Masaya Yoshikai, Takashi Nakamura, Dominic M. Bautista, Eugene C. Herrera, Alvin Baloloy, Rempei Suwa, Basina Ryan, Yasmin H. Primavera-Tirol, Ariel C. Blanco, Kazuo Nadaoka, Field measurement and prediction of drag in a planted rhizophora mangrove forest, J. Geophys. Res. Oceans 127 (11) (2022), https://doi.org/10.1029/2021JC018320 e2021JC018320.
[62] Raúl J. Osorio, Anna Linhoss, Padmanava Dash, Evaluation of marsh terraces for wetland restoration: a remote sensing approach, Water 12 (2) (2020) 336.